Trans Indian Inst Met (2018) 71(2):327–337
https://doi.org/10.1007/s12666-017-1163-1

TECHNICAL PAPER

Vickers Microhardness Studies on B_4C Reinforced/Unreinforced Foamable Aluminium Composites

Arif Uzun[1] · Elif Asikuzun[2] · Ugur Gokmen[3] · Hanifi Cinici[4]

Received: 7 January 2017 / Accepted: 13 June 2017 / Published online: 30 June 2017

Abstract In this work we have investigated the effects of production processes on the structural and mechanical properties of B_4C reinforced/unreinforced foamable aluminium composite materials. All samples were produced with the powder metallurgy method. The production method included compression, extrusion and rolling processes. The Vickers microhardness test was applied to determine the mechanical properties of the samples. Vickers microhardness, elastic modulus and yield strength values of the samples were separately calculated and compared with each other. The experimental microhardness results were analysed using Meyer's law, the proportional sample resistance model, the elastic–plastic deformation model and the Hays Kendall (HK) approach. The results determined that the HK approach was the most suitable model among the other applied microhardness models.

Keywords Foamable material · Aluminum composite · B_4C · Microhardness

✉ Arif Uzun
auzun@kastamonu.edu.tr

[1] Department of Mechanical Engineering, Kastamonu University, Kastamonu, Turkey

[2] Department of Materials Science and Nanotechnology Engineering, Kastamonu University, Kastamonu, Turkey

[3] Technical Sciences Vocational College, Gazi University, Ankara, Turkey

[4] Department of Metallurgy and Materials Engineering, Gazi University, Ankara, Turkey

1 Introduction

Foamable materials, which are used in the production of metallic foams, are pre-foam preform materials. Their most important features, that are distinct from other composite materials, are that they contain foamable material and have a final shape. After these materials are produced, the contained foamable material undergoes decomposition with the applied thermal process forming gas gaps form. The final material is in metallic foam form. The mechanical and physical properties of the produced metallic foam depends on the mechanical and physical properties of the foamable precursor material. Foamable materials can be produced by using powder metallurgy, the semi-solid melt method, accumulated rolling bonding and friction stir welding methods [1–5]. Researchers produced foamable material and foam using these methods. The production of the foamable material first starts with the mixing of the metal powders (alloy powders, reinforcing elements) and the foaming material powders using the powder metallurgy method [1, 6, 7]. Then, the mixture of powders are compressed using different techniques such as extrusion, pressing or rolling for the production of the foamable material [8, 9]. These processes have a direct impact on the density and foamability of the foam. Therefore, it is important to be very careful during the production process, as any structural defect can negatively affect the subsequent operations. For example, when the foamable materials are produced with insufficient compression pressure, the porosity increases in the structure. In this case, inhomogeneous cellular structures are obtained in post-foaming samples (metal foams). It has been emphasized by Young and Kang [10] that uniform structured foams can be obtained from foamable Al6061 alloy with a porosity below 1% depending on the compression pressure and the

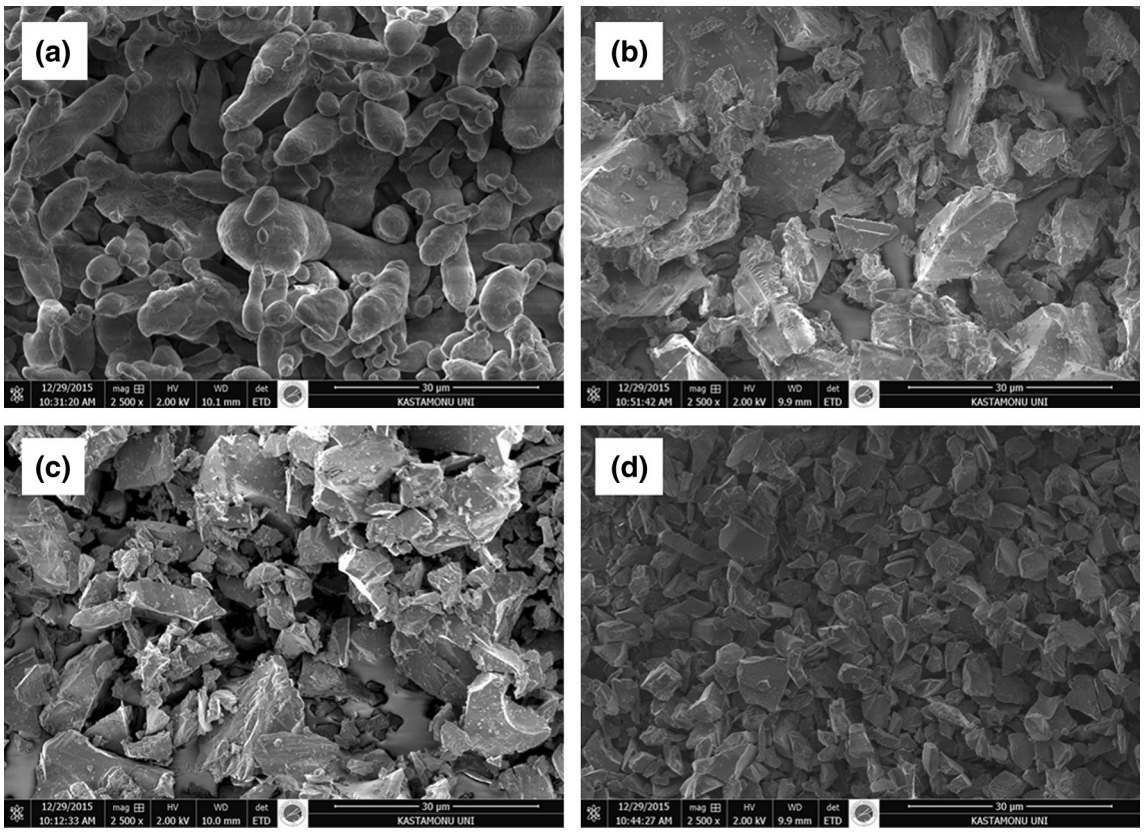

Fig. 1 SEM images of powders used in material production **a** Al, **b** Si, **c** TiH_2, **d** B_4C

heating temperature. Ceramic particles such as SiC, Al_2O_3, TiB_2, B_4C and TiC are commonly added to increase the stability and improve the mechanical properties of Al foam with the powder metallurgy method [11–16].

The aim of this work is to investigate the effects of the production processes on the mechanical properties of B_4C reinforced/unreinforced foamable Al composites which are produced by the powder metallurgy method. The mechanical properties of the samples generated are determined by the Vickers microhardness test method. The Vickers microhardness analyses are performed using Meyer's law, the proportional samples resistance (PSR) model, the elastic/plastic deformation (EPD) model and the Hays-Kendall (HK) approach.

2 Experimental Procedures

2.1 Production of Foamable Aluminum Composite Materials

The foaming material TiH_2 powder (<44 μm) at 1%, alloy element Si powder (<44 μm) at 7% and reinforcement element B_4C powder (<10 μm) at 4% are used into matrix material Al powder (<160 μm) for the production of foamable materials. Powders are mixed by Turbula brand T2 F type three-dimensional mixer for 30 min. SEM images of the powders are shown in Fig. 1.

The mixture powders are uni-directionally cold compressed under 400 MPa by using hydraulic press in steel mould. After compression, cylindrical powder/metal block samples are produced with a diameter of 62 mm and a length of 80 mm. Then, densification process such as extrusion and rolling are applied in order to convert these samples to plates. Firstly, block samples and extrusion mould are heated in the furnace at 550 °C for 1 h for the extrusion process. Then, block samples are placed in the mould and are extruded at a ratio of 1/4. After extrusion, samples that have a cross-sectional area of 25×30 mm^2 are obtained and they are annealed at 550 °C for 20 min using Protherm PLF 120/12 model furnace. Then the rolling process is applied to the samples. Rolling is carried out in five cycles and thus thickness of plate is reduced to 5 mm. The samples are heated at 550 °C for 20 min during each cycle. Strain rates ($\dot{\varepsilon}$) in rolling process are given in Table 1. This ratio can be found out from Eq. 1.

Table 1 Rolling process parameters (total strain, strain rate)

Cycle	Thickness (mm)	Strain rate ($\dot{\epsilon}$)
h_0	30	0
h_1	25	0.18
h_2	20	0.22
h_3	15	0.29
h_4	10	0.41
h_5	5	0.69
	Total	1.79
	Average	0.35

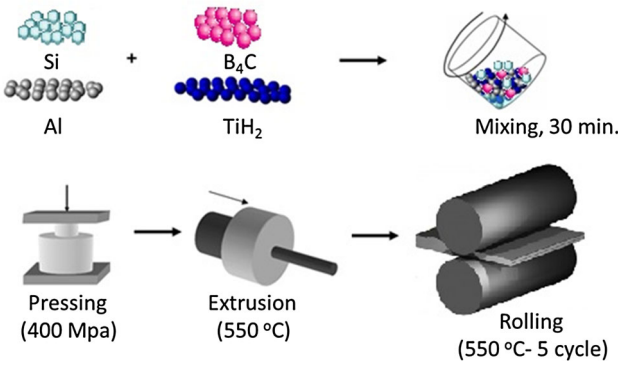

Fig. 2 Schematic diagram of the production process of foamable materials

$$\dot{\epsilon} = ln\left(\frac{h_0}{h_f}\right) \quad (1)$$

Here h_0 and h_f are the thicknesses of the sample before and after rolling, respectively. The production process of the foamable materials is shown in Fig. 2. The images of the samples obtained at each cycle are shown in Fig. 3. During experimental studies, the 4% B_4C reinforced/unreinforced samples are named as B_4 and B_0, respectively.

3 Results and Discussion

3.1 Microstructural Analysis

Figure 4 shows the microstructure of B_4C reinforced/unreinforced foamable aluminium composites produced by the compression, extrusion and rolling processes, according to which the microstructure contains pores and micro-voids at different volume fractions. The pores and micro-voids appear as dark spots shown in black with arrows marking the triple points where the particles are connected to each other. These pores have to be eliminated in order to provide a full density material and improve the mechanical properties. It is clearly seen that the microstructure of the cold compacted sample contains a large amount of pores

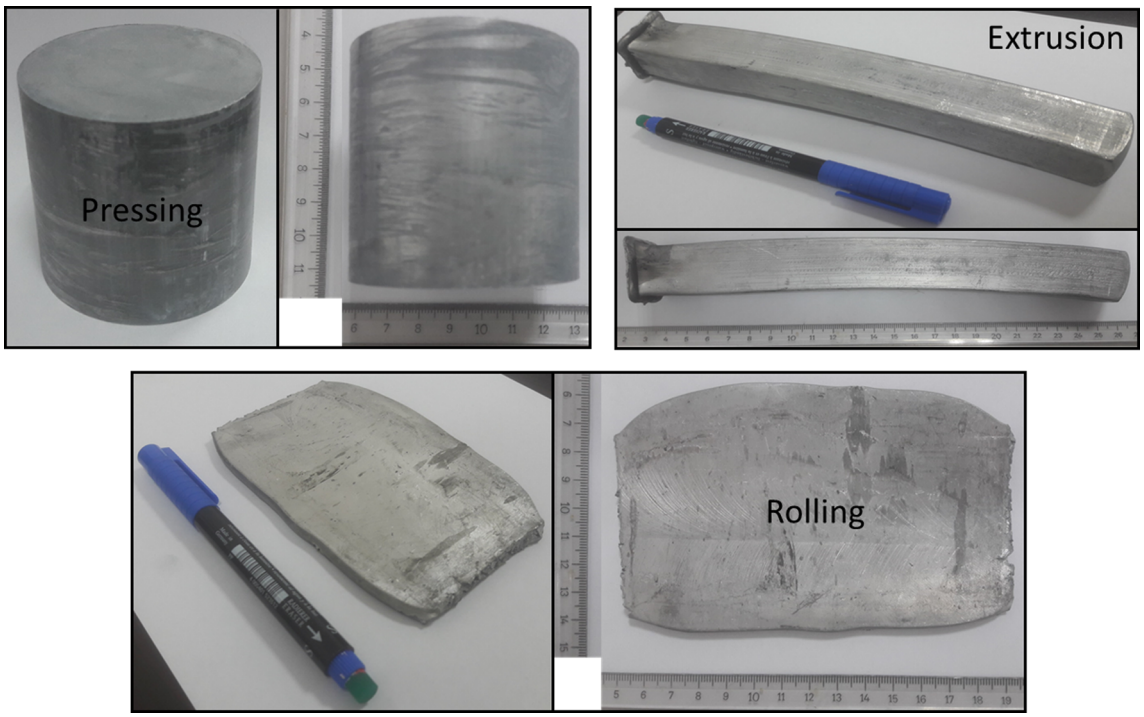

Fig. 3 The samples obtained after pressing, extrusion and rolling process

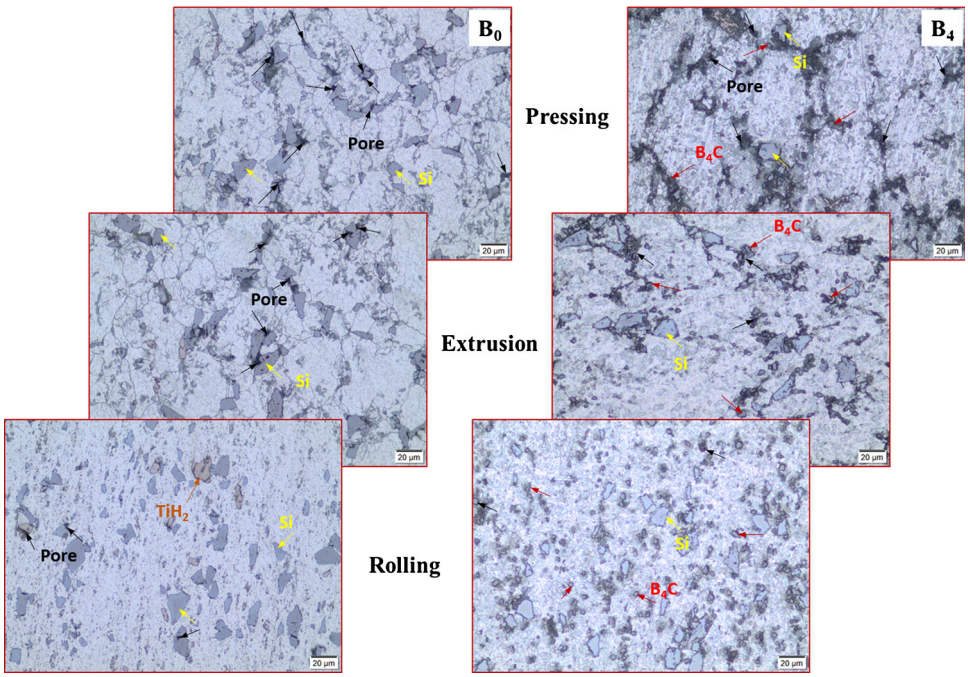

Fig. 4 Microstructure images of the samples after pressing, extrusion and rolling process

Table 2 Relative density of the samples at different period of production process

Samples	Relative density (%)
B_0	
Pressing	94.22
Extrusion	96.44
Rolling	99.65
B_4	
Pressing	92.14
Extrusion	94.60
Rolling	99.54

compared to the extruded and the rolled samples. When high compression pressures are applied to the samples during the extrusion and rolling processes, particle movement is limited and the applied energy is depleted by the plastic deformation of the powders [17, 18]. The relative density of B_4C reinforced/unreinforced foamable aluminium composites are presented in Table 2. The results show that the relative density of B_4C-free compacted samples is only ~94%, and reaches ~96 and ~99% after extrusion and rolling, respectively. On the other hand, the relative density values for the B_4C reinforced samples are relatively low. The relative density of B_4C reinforced compacted sample is ~92%, and reaches ~95 and ~99% after extrusion and rolling, respectively. The increase in the relative density is due to the void/pore reductions and better distribution of B_4C as a result of extrusion and rolling. B_4C particles shown with the red arrows in Fig. 4 get rearranged during the rolling and extrusion operations because the composite materials are subjected to severe deformation caused by high compressive stresses. The voids or pores in the structure are substantially reduced. With the extrusion and rolling processes, the particle agglomeration is reduced and better distribution of particles are obtained. Chen et al. [19] emphasized similar results.

3.2 Vickers Microhardness Measurements

Vickers microhardness measurements are made using a Shimadzu brand HMV-2 model digital microhardness tester at room temperature. Five different loads (0.245, 0.480, 0.980, 1.96 and 2.940 N) are applied to the surface of the materials. Three indentations are taken at each load. It is noted that the traces of the indenter do not overlap during this process. Then, diagonal to the traces is measured using a microscope. The relationship between the Vickers microhardness and load (F)/area of trace (A) is calculated using Eq. 2.

$$Hv = 1854.4\left(\frac{F}{d^2}\right) \tag{2}$$

Here Hv is the Vickers microhardness, F is the applied load and d is the diagonal length of the indentation. In addition, the load dependent elastic modulus (E) and yield strength (Y) values are calculated using Eqs. (3) and (4) for all samples.

Table 3 Load-dependent *Hv*, *E* and *Y* values of the samples

Samples	F (N)	(1) H_v (GPa)	(2) H_v (GPa)	(3) H_v (GPa)	SD standard deviation	H_v (GPa) mean	E (GPa)	Y (GPa)
B_0								
Pressing	0.245	0.331	0.291	0.327	0.022	0.316	25.892	0.105
	0.490	0.387	0.344	0.353	0.022	0.361	29.589	0.120
	0.980	0.433	0.411	0.384	0.024	0.409	33.502	0.136
	1.960	0.418	0.412	0.432	0.010	0.421	34.492	0.140
	2.940	0.404	0.413	0.393	0.010	0.403	33.0511	0.134
Extrusion	0.245	0.318	0.334	0.386	0.036	0.344	28.216	0.114
	0.490	0.329	0.395	0.426	0.050	0.380	31.141	0.126
	0.980	0.387	0.470	0.462	0.046	0.437	35.844	0.145
	1.960	0.427	0.442	0.452	0.013	0.440	36.080	0.146
	2.940	0.432	0.420	0.441	0.011	0.431	35.328	0.143
Rolling	0.245	0.340	0.359	0.439	0.053	0.376	30.825	0.125
	0.490	0.441	0.420	0.463	0.021	0.441	36.109	0.146
	0.980	0.483	0.515	0.541	0.029	0.512	41.958	0.170
	1.960	0.458	0.543	0.512	0.043	0.503	41.193	0.167
	2.940	0.490	0.512	0.529	0.019	0.510	41.786	0.169
B_4								
Pressing	0.245	0.327	0.340	0.335	0.006	0.334	27.361	0.111
	0.490	0.370	0.387	0.363	0.012	0.373	30.564	0.124
	0.980	0.487	0.459	0.399	0.045	0.446	36.542	0.148
	1.960	0.433	0.446	0.445	0.007	0.442	36.191	0.147
	2.940	0.447	0.436	0.468	0.016	0.450	36.894	0.150
Extrusion	0.245	0.325	0.349	0.358	0.017	0.344	28.161	0.114
	0.490	0.413	0.414	0.408	0.003	0.412	33.758	0.137
	0.980	0.456	0.443	0.482	0.020	0.459	37.580	0.152
	1.960	0.462	0.456	0.457	0.003	0.459	37.619	0.152
	2.940	0.461	0.440	0.474	0.017	0.458	37.566	0.152
Rolling	0.245	0.475	0.411	0.424	0.034	0.435	35.678	0.145
	0.490	0.479	0.438	0.420	0.030	0.445	36.445	0.148
	0.980	0.490	0.511	0.499	0.011	0.500	40.983	0.166
	1.960	0.495	0.503	0.535	0.021	0.511	41.855	0.170
	2.940	0.505	0.500	0.508	0.004	0.504	41.346	0.168

$$E = 81.9635\,Hv \tag{3}$$

$$Y \approx \frac{Hv}{3} \tag{4}$$

The results that are obtained from the experimental studies are shown in Table 3. It can be seen from the table that the microhardness of materials depends on the applied load. When variation of the microhardness values is taken into consideration, the importance of the different compression methods applied is better understood. The reverse indentation size (RISE) effect is observed in all samples. So, the microhardness values increase with increasing applied load. Elastic modulus (*E*) and yield strength (*Y*) are important parameters to characterize the mechanical properties of materials. The elastic modulus refers to the elastic behaviour of the material under load. More force is needed to change the shape of a rigid material. In this case, the elastic modulus of the material is large. Increasing values of *Hv* and *E* shows that more force must be applied to change the shape of the material. The formability of the material is seen to increase after extrusion and rolling of the pressed sample. According to the previous studies, the reason behind this is an increase in the ratio of relative intensity that is formed with pressing. Samples are deformed by the effect of radial and angular forces during the extrusion and rolling processes

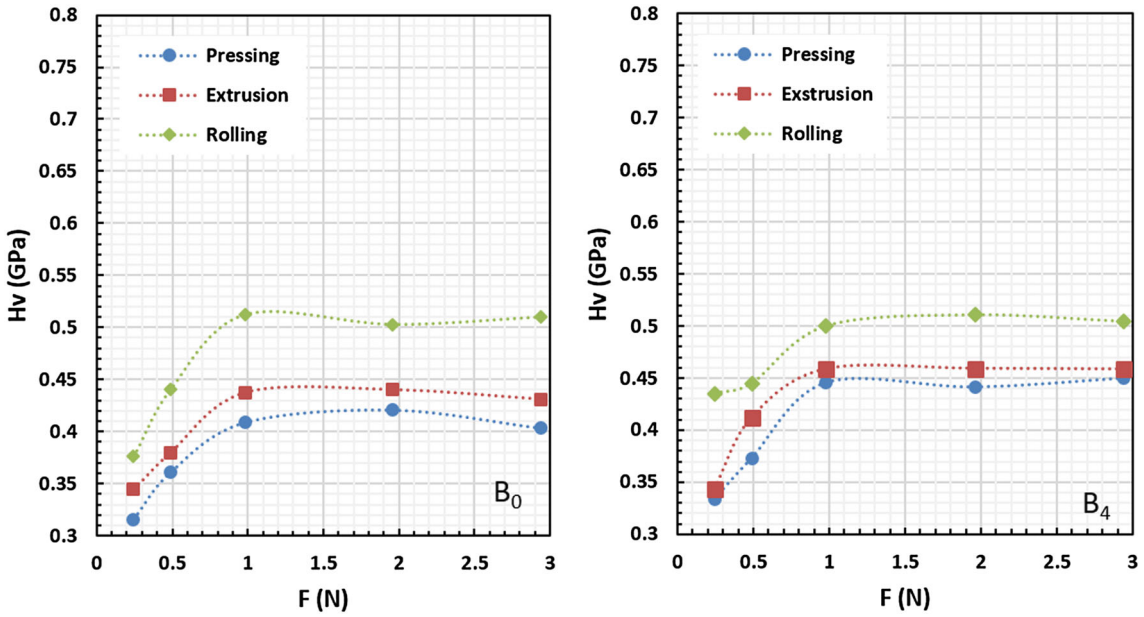

Fig. 5 Variations of load-dependent micro hardness in the samples

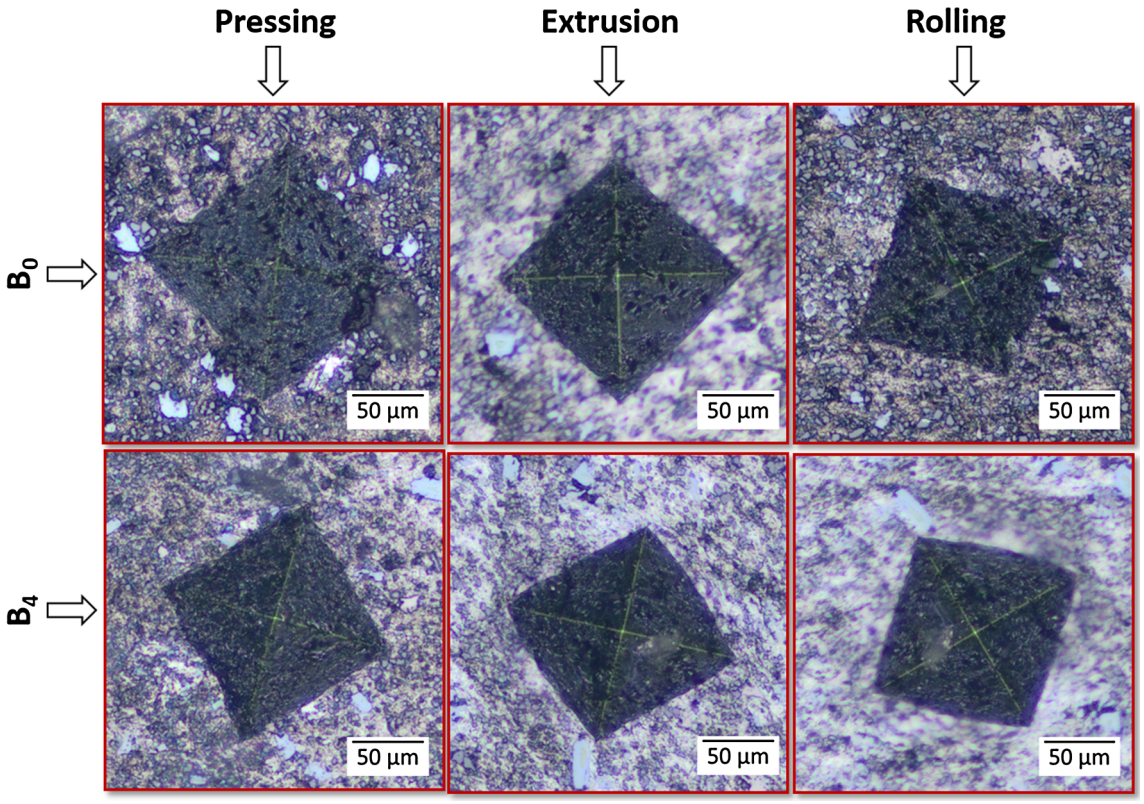

Fig. 6 The optical trace photos under 2.940 N load for the samples

and in this way, more dense structures are obtained by eliminating structural pores [16]. A similar situation occurs in each of the two sample types (Fig. 4). Microhardness values of the B_4 samples are greater than the B_0 samples. The reason for this is that, hard B_4C samples cause stress in the matrix [20]. The microhardness increases with increasing deformation. So there is an increase in E and Y values in both the samples. This is an expected result as the E and Y values depend on microhardness.

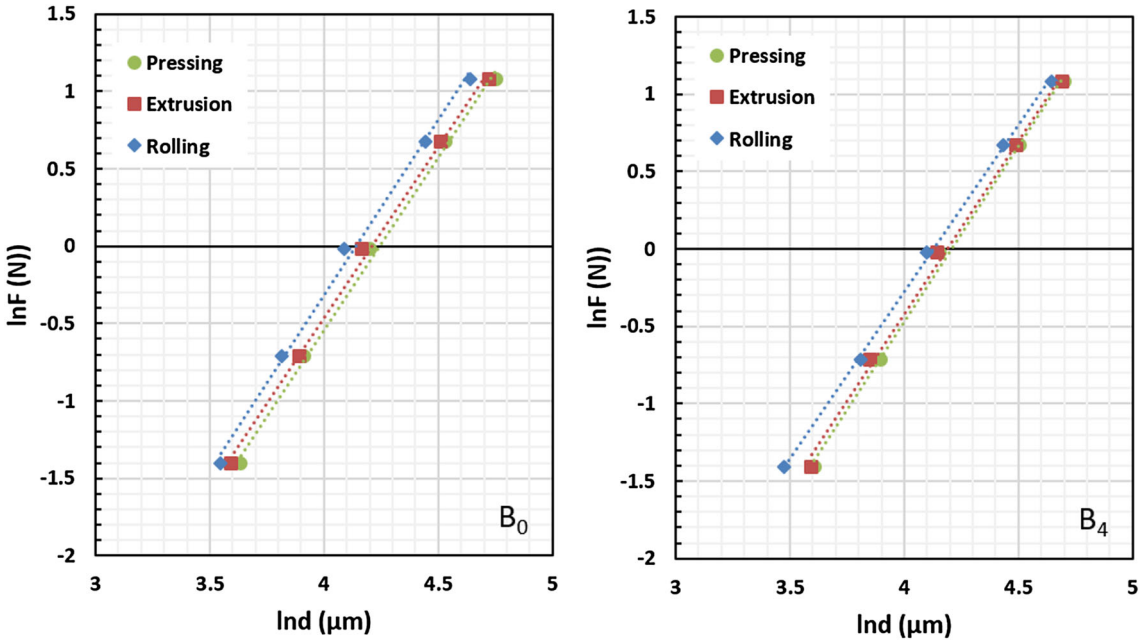

Fig. 7 Variation of applied load *lnF* with diagonal *lnd* for the samples

Table 4 Best-fit results of experimental data according to Meyer's law

Samples	n_K	In A_{1K}	H_v (GPa)
B_0			
Pressing	2.217	−9.469	0.403–0.421
Extrusion	2.198	−9.306	0.431–0.440
Rolling	2.279	−9.493	0.503–0.510
B_4			
Pressing	2.273	−9.609	0.442–0.450
Extrusion	2.262	−9.536	0.459–0.459
Rolling	2.126	−8.795	0.504–0.511

The graph of microhardness against the applied load is given in Fig. 5. As can be seen from the graph, microhardness values increases with increasing applied load from 0.245 to 2.940 N. Moreover, a plateau region is reached at around 1 N and a significant change in the microhardness values is not observed over 1 N. The optical trace photos of the indentations for each sample are shown in Fig. 6 under 2.940 N load. No cracks are observed on either sample. This shows that the samples exhibit ductile behaviour instead of brittle behaviour.

3.3 Analyses and Models

3.3.1 Meyer's Law

Meyer's law, which is an expression of a simple experiment, has been developed to explain the ISE (indentation size effect) or RISE (reverse indentation size effect) behaviour of materials and it indicates the relationship between the applied load and the trace. Meyer's law, which is a simple load law, is given in Eq. 5.

$$F = Ad^{n_K} \tag{5}$$

Here A is a standard hardness constant and Meyer's number n is a measure of the ISE or RISE. If the n value is greater than 2, the RISE behaviour is obtained. If the n value is less than 2, the ISE behaviour is obtained. These data are procured by fitting of the graphs obtained from the experimental data. The n values, which are obtained from the slope of the *InF–Ind* graph (Fig. 7), are greater than 2 for all samples. The obtained results are shown in Table 4. These results confirm that the load-dependent displacement behaviour of the analysed samples is RISE behaviour.

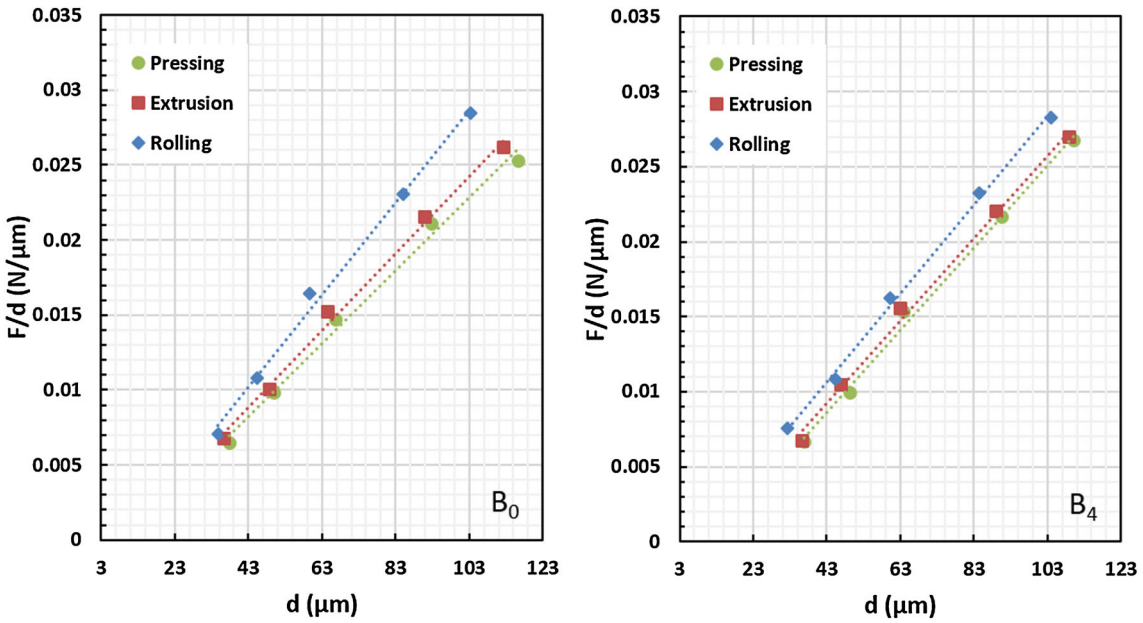

Fig. 8 Plots of F/d versus d for the samples

Table 5 Best-fit results of experimental data according to PSR model

Samples	$\beta \times 10^{-4}$ (N/μm^2)	H_{PSR} (GPa)	$\alpha \times 10^{-4}$ (N/μm)	H_v (GPa)
B_0				
Pressing	2.40	0.445	−26.5	0.403–0.421
Extrusion	2.54	0.472	−25.1	0.431–0.440
Rolling	3.11	0.577	−37.7	0.503–0.510
B_4				
Pressing	2.74	0.508	−34.8	0.442–0.450
Extrusion	2.78	0.515	−33.7	0.459–0.459
Rolling	2.88	0.535	−17.4	0.504–0.511

3.3.2 Proportional Sample Resistance (PSR) Model

PSR is a model used for microhardness analysis of materials that exhibit ISE behaviour in general [9]. The equation for the model is given below.

$$\frac{F}{d} = \alpha + \beta d \tag{6}$$

Here the α and β values are calculated from the graph *(F/d)–d* shown in Fig. 8. The change of the α value is related to surface cracks [21]. In the *PSR* model, the load-independent microhardness values are calculated (Eq. 7).

$$H_{PSR} = 1854.4\beta \tag{7}$$

As can be seen from Table 3, the value of α is negative for all samples. This is an indication of RISE behaviour. This situation confirms that only plastic deformation occurs in these samples. In other words, no elastic deformation is observed for the applied loads. There is no voltage discharge on the sample after the indenter is removed from the sample surface. Therefore, the microhardness of the material increases. When the microhardness values, which are obtained according to the *PSR* model, are analysed, we can see that the microhardness values are quite far from the plateau region (Table 5). As a result, this model is not sufficient for the determination of the actual hardness.

3.3.3 Elastic/Plastic Deformation (EPD) Model

According to the elastic/plastic deformation model (*EPD*), the relationship between the applied load and trace is given in the following Eq. (8) [21–27].

$$F = A_2\left(d_p + d_e\right) \tag{8}$$

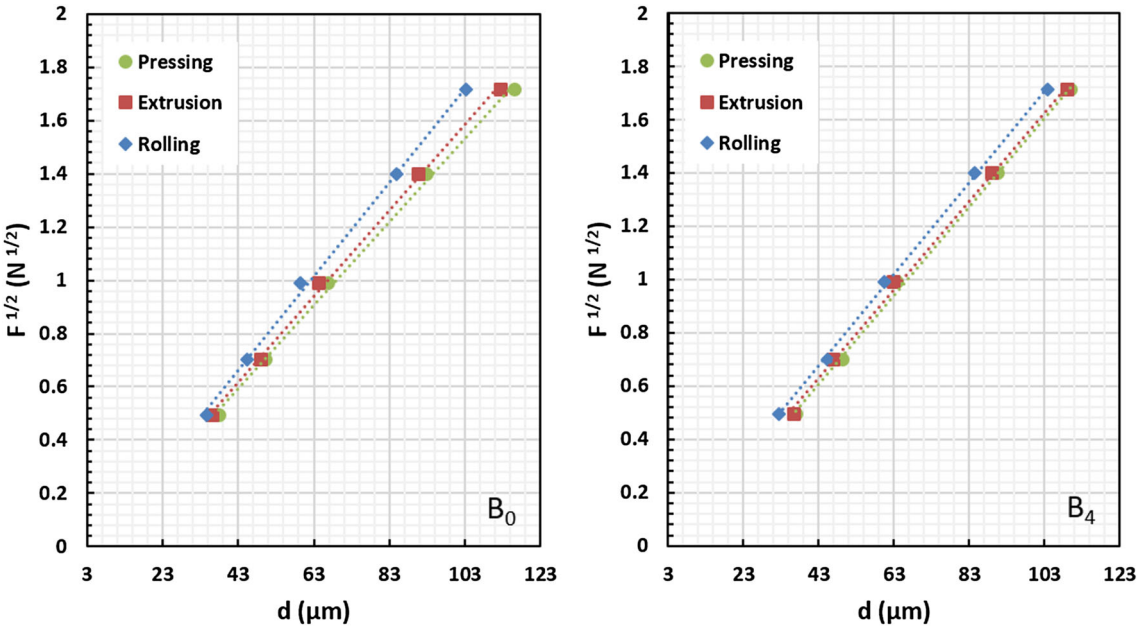

Fig. 9 Plots of diagonal length versus square root of applied loads for the samples

Table 6 Best-fit results of experimental data according to EDP model

Samples	A_2 (N/μm^2)	d_e (μm)	H_{EPD} (GPa)	H_v (GPa)
B_0				
Pressing	0.0155	−0.0798	0.449	0.403–0.421
Extrusion	0.0160	−0.0764	0.475	0.431–0.440
Rolling	0.0177	−0.0977	0.585	0.503–0.510
B_4				
Pressing	0.0166	−0.1085	0.515	0.442–0.450
Extrusion	0.0167	−0.0871	0.521	0.459–0.459
Rolling	0.0170	−0.0612	0.537	0.504–0.511

Here A_2 is a constant, d_e is related to the plastic deformation (d_p). A_2 and d_e values can be calculated from the graph of $F^{(1/2)}$–d_p (Fig. 9). In this model, the load-independent microhardness value is calculated from Eq. 9.

$$H_{EPD} = 1854.4A_2 \tag{9}$$

When this model is applied, as seen in Table 6, the d_e value found from the point where the graph intersects the y axis is negative for all samples because there is no elastic deformation for the applied loads. This result is evidence of the RISE behaviour of the material.

3.3.4 Hays Kendall Approach

Hays and Kendall suggested that the minimum load value (W) can create permanent deformation in a sample [28]. If the applied load does not exceed the resistance of the sample, plastic deformation does not occur. Only elastic deformation occurs on the sample surface. Hays-Kendall explained that the diagonal length of the trace (d) is associated with an effective load (F_{eff}) instead of the applied test load (F) (Eq. 10).

$$F_{eff} - W_{HK} = A_{HK}d^2 \tag{10}$$

Here A_{HK} is a constant independent of the applied load. W and A_{HK} values are obtained from the graph F–d^2 given in Fig. 10. Load-independent microhardness values are calculated from the following equation.

$$H_{HK} = 1854.4A_{HK} \tag{11}$$

In Table 7, the values of W_{HK}, A_{HK} and H_{HK} are summarized. As can be seen from the table, the W_{HK} values are negative for all samples. This is a result of RISE behaviour.

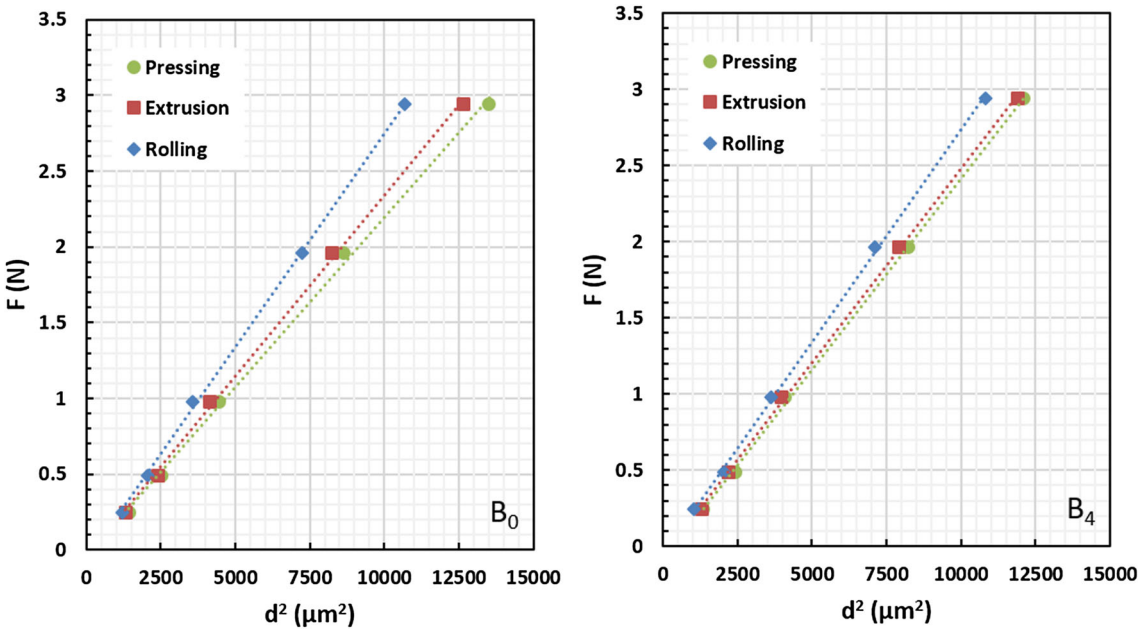

Fig. 10 Applied load versus the square of the impression semi-diagonal length for the samples

Table 7 Best-fit results of experimental data according to HK model

Samples	$A_{HK} \times 10^{-4}$ (GPa)	W_{HK} (N)	H_{HK} (GPa)	H_v (GPa)
B_0				
Pressing	2.2	−0.075	0.413	0.403–0.421
Extrusion	2.3	−0.068	0.441	0.431–0.440
Rolling	2.8	−0.098	0.526	0.503–0.510
B_4				
Pressing	2.5	−0.096	0.464	0.442–0.450
Extrusion	2.5	−0.092	0.472	0.459–0.459
Rolling	2.7	−0.043	0.511	0.504–0.511

So, it can be concluded that the applied load is sufficient for plastic deformation. As a result, the microhardness values, which are calculated using the Hays-Kendall model, are relatively compatible with the microhardness values in the plateau region.

4 Conclusions

In this study, the Vickers microhardness measurements are performed to determine the effects of secondary processes applied to 4% B_4C reinforced/unreinforced foamable materials produced by the powder metallurgy method on the mechanical properties. The results are analysed with the Meyer's law, PSR, EPD models and the Hays-Kendall approach. The following results are obtained:

- Vickers microhardness values increases with increasing deformation rate.
- The load-dependent elastic modulus and yield strength values of the samples are at maximum levels during rolling compared to those during the pressing process.
- All samples prepared follows RISE behaviour. The microhardness values increases with increasing applied load.
- As a result, it can be concluded that the Hays-Kendall approach is the most suitable model among the other applied microhardness models.

Acknowledgements This study was funded by the Kastamonu University, Scientific Research Projects Coordination Department, Kastamonu, Turkey (Project Number: KÜBAP-01/2014-11).

References

1. Banhart J, *JOM-J Min Met Mater Soc* **52** (2000) 22.

2. Hangai Y, and Utsunomıya T, *Metall Mater Trans A* **40** (2009) 275.
3. Kitazono K, Kikuchi Y, Sato E, and Kuribayashi K, *Mater Lett* **61** (2007) 1771.
4. Gergely V, and Clyne B, *Adv Eng Mater* **2** (2000) 175.
5. Li N, Xing S, Bao P, and Liu Z, *A research on fabrication of aluminum foam precursor using semi-solid melt*, Proc. 2nd International Conference on Mechanical and Electronics Engineering (ICMEE 2010), Kyoto, Japan, August 2010, p 49.
6. Banhart J, *Prog Mater Sci* **46** (2001) 559.
7. Banhart J, *MRS Bull* **28** (2003) 290.
8. Baumgärtner F, Duarte I, and Banhart J, *Adv Eng Mater* **2** (2000) 168.
9. Degischer H P, and Krıszt B, *Handbook of Cellular Metals: Production, Processing and Applications*, Weinheim, Wiley (2002), p 1.
10. Young S W, and Kang C G, *Metall Mater Trans B* **35B** (2004) 769.
11. Asavavisithchai S, and Opa A, *Chiang Mai J Sci* **37** (2010) 213.
12. Gokmen U, and Turker M, *J Fac Eng Archit Gazi Univ* **27** (2012) 651.
13. Güden M, and Yüksel S, *J Mater Sci* **41** (2006) 4075.
14. Kennedy A R, and Asavavisitchai S, *Adv Eng Mater* **6** (2004) 400.
15. Kennedy A R, and Asavavisitchai S, *Scri Mater* **50** (2004) 115.
16. Uzun A, and Turker M, *Int J Mater Res* **106** (2015) 970.
17. Varol T, and Canakci A, *Met Mater Int* **19** (2013) 1227.
18. Hafizpour H R, Simchi A, and Parvizi S, *Adv Powder Technol* **21** (2010) 273.
19. Chen H S, Wang W X, Nie H H, Li, Y L, Wu Q C, and Zhang P, *Acta Metall Sin (Engl Lett)* **28** (2015) 1214.
20. Abdullah Y, Yusof M R, Muhammad A, Kamarudin N, Paulus W S, Shamsudin R, Shudin N H, and Zali N M, *J Nucl Relat Technol* **9** (2012) 42.
21. Li H, and Bradt R C, *J Mater Sci* **28** (1993) 917.
22. Bull S J, Page T F, and Yoffe E H, *Philos Mag Lett* **59** (1989) 281.
23. Quinn J B, and Quinn G D, *J Mater Sci* **32** (1997) 4331.
24. Ozturk O, Cetinkara H A, Asıkuzun E, Akdogan M, Yilmazlar M, and Terzioglu C, *J Mater Sci Mater Electron* **22** (2011) 1501.
25. Asikuzun E, Ozturk O, Cetinkara H A, Yildirim G, Varilci A, Yılmazlar M, and Terzioglu C, *J Mater Sci Mater Electron* **23** (2012) 1001.
26. Tosun M, Ataoglu S, Arda L, Ozturk O, Asikuzun E, Akcan D, and Cakiroglu O, *Mater Sci Eng A Struct* **590** (2014) 416.
27. Upit G P, and Varchenya S A, *Phys Status Solidi B* **17** (1966) 831.
28. Hays C, and Kendall E G, *Metallography* **6** (1973) 275.